Bagheri, M.; Masoomi, MY.; Domínguez Torres, E.; García Gómez, H. (2021). High hydrogen release catalytic activity by quasi-MOFs prepared via post-synthetic pore engineering. Sustainable Energy & Fuels. 5(18):4587-4596. https://doi.org/10.1039/d1se00661d

Journal Name

ARTICLE

High Hydrogen Release Catalytic Activity by Quasi-MOF Prepared via Post-Synthetic Pore Engineering

Received 00th January 20xx,
Accepted 00th January 20xx

DOI: 10.1039/x0xx00000x

www.rsc.org/

Minoo Bagheri[a], Mohammad Yaser Masoomi[a]*, Esther Domínguez,[b] and Hermenegildo García[b*]

The catalytic activity of metal-organic framewroks (MOFs) depends largely on the presence of structural defects. In the present stuyd, cobalt based metal-organic framework TMU-10, $[Co_6(oba)_5(OH)_2(H_2O)_2(DMF)_4]_n{\cdot}2DMF$ has been submitted under controlled conditions to thermolysis under air atmosphere at different temperatures in the range of 100-700 °C. This treatment produces the removal of ligands, generation of structural defects and additional porosity in a controlled way. The resulting materials, denoted according to the literature as *quasi* MOFs, were subsequently employed as catalysts for hydrogen generation from $NaBH_4$ by hydrolysis. The quasi TMU-10 framework obtained at 300 °C (QT-300) shows the highest turnover frequency of the series with a value of 13333 $mL.min^{-1}g^{-1}$ at room temperature in the absence of base, with an activation energy of 56.8 kJ×mol^{-1}. The simultaneous presence of micro- and mesopores in QT-300 with unsaturated Lewis acid sites on cobalt nodes due to the conversion of a fraction of Co(II) centers to Co(III) as well as the presence of tetrahedral Co(II) sites are responsible for this catalytic behavior. Influence of catalyst dosage and BH_4^- concentration is in good agreement with the Langmuir Hinshelwood model in which both reactants must be adsorbed on to the catalyst surface. Further investigation on hydrolysis of the $NaBH_4$+D_2O system presents a primary kinetic isotope effect indicating that water O-H bond cleavage occurs in the rate determining step.

Introduction

The replacement of fossil fuel with clean and economically-viable renewable fuels is attracting a considerable attention especially in chemistry and material sciences. Green hydrogen from water is one of the best options as renewable electricity storage into chemicals and energy vector due to the high specific mass energy density of 120 MJ kg $^{-1}$ which is higher than those of diesel and gasoline (46 MJ kg $^{-1}$) and the environmental innocuous by-products. [1, 2] H_2 production from water by electrolysis [3], thermolysis [4, 5], water splitting [6, 7] and photocatalytic water splitting,[7-10] chemocatalytic hydrogen generation reactions (HGR) are also of interest as a procedure for *on-demand* fast H_2 release from a liquid or solid phase.[2] Among chemocatalytic HGR, catalytic hydrolysis of hydrides is one of the most studied process to the mild conditions and high H_2 release rate.[11] Among them, $NaBH_4$ is one of the most favorable and convenient chemical hydrogen storage substances due to its acceptable H_2 capacity (10.8 wt.%), high released H_2 purity, manageable H_2 production rate, high stability in alkaline solution, as well as safe and pollution-free characteristics.[12] Hydrolysis of $NaBH_4$ produces 4 moles of H_2 under mild conditions, which has a much higher efficiency than other H_2 storage compounds that have been studied. [13, 14] However, the hydrolysis is kinetically slow and a proper catalyst is required to enhance and control the rate of the HGR.[15] Most studies have been reported expensive and rare noble catalysts, such as ruthenium and platinum.[16-20] Therefore, other affordable and multi-purpose catalysts with high stability and efficiency are highly required.

In the past two decades, the use of metal organic frameworks (MOFs) as solid catalysts has expanded significantly due to the flexibility in the composition, the large variety of crystalline porous frameworks, the well-defined structure of the active sites, the ability to design the structure with desired chemical components to adjust proper performance and high surface area along with capability of pore engineering. [21-25] The number of reports on the use of MOFs as catalysts for the chemocatalytic HGR is still scarce mainly due to inaccessibility of active sites.[26, 27] To overcome this problem, pore engineering by producing coordinatively unsaturated metal active sites has been suggested.[28]

Generation of defects in MOFs is a well-proven strategy to increase the catalytic activity and increase porosity. Besides removal of the coordinated solvent molecule,[29, 30] controlled thermal removal of ligand (“*deligandation”*) has been reported to create the Lewis acid centers. [31, 32] Very recently, the term Quasi-MOFs (Q-MOFs) has been proposed to indicate those MOFs submitted to controlled thermal treatment that could represent a bridge between MOFs and metal compounds (such as metal oxides, nitrides, sulfides, and phosphides) have

*Corresponding authors
a. Department of Chemistry, Faculty of Science, Arak University, Arak 3848177584, Iran
E-mail: m-masoomi@araku.ac.ir
b. Instituto Universitario de Tecnología Química, Universitat Politecnica de Valencia-Consejo Superor de Investigaciones Científicas, Av. De los Naranjos s/n, 46022 Valencia, Spain. E-mail: hgarcia@upv.es
c. Electronic Supplementary Information (ESI) available: Additional characterization data, reaction setup and temporal H_2 evolution profiles and other catalytic activity of QT-300. See DOI: 10.1039/x0xx00000x

received special attention. Q-MOFs are obtained by controlled thermal deligandation process.[33-36] By partial deligandation not only the intrinsic specific surface area is maintained or even increased, but also the generation of hierarchical micro and mesopores favouring diffusion can be observed. Hierarchical porosity can facilitate diffusion of substrates to and products from the active centres, increasing the reaction rate.[37] All these features of Q-MOFs can lead to an enhanced catalytic activity respect to the parent MOF. [34, 38] The partial thermolysis of MOFs may also result in the formation of small metal or metal oxide particles inside a material of hierarchical pores, while maintaining in general the crystallinity of a framework.

We herein report the improved HGR activity of a cobalt Q-MOF catalyst, derived from TMU-10 due to the generation of extra high density open metal sites and the simultaneous formation of both micro- and mesopores after partial thermal deligandation treatment. In other words, controlled thermal treatment creates highly active sites and separate particles occluded within the whole network of QTMU-10 along with the simultaneous presence of micro- and mesopores. In contrast to most reported metal oxide systems,[39, 40] and in order to obtain an improved catalytic H_2 release material, the present study reports that effective partial deligandation originates active metal sites, while avoiding particle aggregation inside a MOF framework having simultaneously micro- and mesopores. In the modified Q-MOF, the porosity and skeleton structure of the parent TMU-10 were maintained in some extent, ensuring reactant access to the active sites as well as their easier diffusion through the material.

Up until now defective MOFs with ligand vacancies in their framework have been studied as improved catalysts in CO oxidation involving reactive oxygen species, [34, 41-43] CO_2 adsorption [33] and oxidation of benzyl alcohol.[44] To the best of our knowledge, there has been no previous report on the use of Q-MOFs in the catalytic hydrogenation under mild conditions.

TMU-10, $[Co_6(oba)_5(OH)_2(H_2O)_2(DMF)_4]_n$·2DMF ($H_2$oba = 4,4′-oxybisbenzoic acid), is a Co based MOF with high thermal stability in which there are hexanuclear secondary building units (SBUs) of cobalt centers as non-noble catalyst..[45] Herein, it will be described how partial deligandation on TMU-10 can produce a highly active non-noble H_2 release Q-MOF catalyst (abbreviated as "QT-x" in this study), consisting of coordinatively unsaturated Lewis acid sites, as well as coexistence of micro- and mesopores. The Q-MOF has been obtained by controlled thermal treatment in air at various temperatures to partially remove organic ligand for adjusting the Lewis acid strength of Co nodes to the requirements of the reaction. The catalytic activity of QTMU-10 dramatically changes with its deligandation temperature. The highest catalytic HGR performance was observed for deligandation treatment at 300 ºC, probably due to simultaneous presence of micro- and mesopores as well as the uniform and extended distribution of active cobalt catalytic sites across the framework and prevention of particle agglomeration. Its reusability and the corresponding kinetics and thermodynamic properties were also investigated. The catalytic activity of QT-300 was also compared to that of TMU-10 precursor and Co_3O_4 residual. Our findings indicate that QTMU-10 can construct a porous structure and a strong interaction between the guest and cooperative multisite catalysis sites (pores and unsaturated metal sites), which cannot be achieved in its related MOF and metal oxide.

Experimental

Materials and Physical Techniques.

All reagents and materials for the synthesis and analysis were commercially available from Aldrich and Merck Company and used without further purification. IR spectra were recorded using Thermo Nicolet IR 100 FT-IR. PL-STA 1500 apparatus was used for measurement of thermal behavior, heating the samples at the rate of 10 ºC min^{-1} in a static nitrogen atmosphere. Powder X-ray diffraction (PXRD) measurements were performed by a Philips X'pert diffractometer with monochromated Cu-K_α radiation. Elemental analyses were collected on a CHNS Thermo Scientific Flash 2000 elemental analyzer. Sorption studies of N_2 at 77 K were performed using the TriStar II 3020 surface area analyzer from Micrometrics Instrument Corporation and BELSORP-mini II from LMS Instruments Co., Ltd. All samples were activated at 120 °C for 14 h under vacuum before N_2 adsorption. The pore-size distributions were calculated from the adsorption branch of the N_2 isotherms according to the BJH method. X-ray photoelectron spectroscopy (XPS) measurements were conducted on a BesTec (Germany) X-ray photoelectron spectrometer with an Al K_α source. The samples were characterized with a field emission scanning electron microscope (FE-SEM) TESCAN MIRAIII (Czech). The leaching of cobalt from QT-300 sample in water was calculated by ICP at the end of the HGR. A powder sample of QT-300 (5 mg) was digested with NaOH (2.5 mL, 2 M) and the resulting clear solution was diluted to 100 mL and adjusted to a pH of 7 with HCl. A simultaneous inductively coupled plasma-optical emission spectrometry (ICP-OES, Varian Vista-PRO, Springvale, Australia) with a radial torch coupled to a concentric nebulizer and Scott spray chamber and equipped with a charge-coupled detector (CCD) was used for ICP measurements. Temperature-programmed desorption of NH_3 (NH_3-TPD) was measured using the Micromeritics TPD-TPR 2900 system equipped with a thermal conductivity detector (TCD). First, the desired amount of the catalyst was pretreated at 150 °C in He stream of 20 mL min^{-1} for 1 h, then cooled down up to 40 °C, and subsequently exposed to ammonia (4 vol.% in He, 20 mL min^{-1}) for 1 h. Then, the ammonia that does not bind to the catalyst was removed by additional purging with 20 mL min^{-1} of He within 30 min. Eventually, the desorption was performed by raising the temperature from 40 to 750 °C at a heating rate of 10 °C min^{-1} in He stream (20 mL min^{-1}).

Synthesis of $[Co_6(oba)_5(OH)_2(H_2O)_2(DMF)_4]_n$·2DMF (TMU-10)

In a typical experiment powder sample of TMU-10 was obtained by mixing oba (2 mmol) and $Co(NO_3)_2.6H_2O$ (0.578 g, 2 mmol) in 40 ml DMF in a round bottom flask at 145 °C for 72 h. The resulting powder was isolated by centrifugation, washed 3 times with DMF and dried in air before characterization. Yield: 0.841 g (89 % based on oba ligand). IR data (KBr pellet, ν/cm^{-1}): 658(m), 782(m), 873(m), 1012(w), 1098(m), 1160(m), 1237(vs), 1398(vs-br), 1504(m), 1558(s), 1603(vs), 1661(vs), 2928(w) and 3417(w-br) (Fig. S1). Elemental analysis (%) calculated for $[Co_6(C_{14}O_5H_8)_5(OH)_2(H_2O)_2(C_3NOH_7)_4]\cdot(C_3NOH_7)_2$: C: 49.3, H: 4.1, N: 3.9; Found: C: 49.6, H: 3.9, N: 3.6.

Synthesis of QT-x samples

In order to obtain the desired quasi MOFs, deligandation of TMU-10 was carried out by thermal treatment in air at a heating rate of 5 °C min^{-1} between 100 and 700 °C for a period of 1 h. The samples were denoted by QT-x, where "T" and "x" stand for TMU-10 and the temperature of thermal treatment, respectively.

Catalytic HGR of QT-x samples

The H_2 evolved in the $NaBH_4$ hydrolyses catalyzed by the QT-x samples was determined according to water-displacement method. [46] In these HGRs, a mixture of the desired amount of catalyst and distilled water was placed in a two-necked round-bottomed flask (100 mL), which was put in a water bath at room temperature under ambient atmosphere. A gas burette filled with water was connected to the reaction flask to evaluate the H_2 volume. To start the catalytic HGR, an aqueous $NaBH_4$ solution at the required concentration was injected into the mixture using a syringe (Fig. S2). HGR starts immediately when the $NaBH_4$ solution was in contact with QT-x catalyst. The HGR efficiency was determined by measuring the volume of H_2 via recording the water displacement in the gas burette. The reaction was completed when no more H_2 gas was generated. The turnover frequency (TOF) (ml H_2 g cat^{-1} min^{-1}) was calculated as follows:

$$\mathrm{TOF} = \frac{V_{H_2O}}{t.m_{cat}} \qquad (1)$$

where V_{H_2O} (mL) corresponds to the water volume (mL) displaced by H_2 gas in time (t), and m_{cat} refers to the catalyst weight in grams. Additionally, kinetics studies were carried out using different concentrations of $NaBH_4$ and catalyst dosages. The experiments were performed at different temperatures (25, 35, 40 and 45 °C) to determine the apparent activation energy as follows:

$$\ln k = \ln A - \frac{E_a}{RT} \qquad (2)$$

Where k in mL H_2 min^{-1} g^{-1} denotes the catalytic HGH rate, A is the pre-exponential factor, R (8.314 J mol^{-1} K^{-1}) is gas constant, and T in K is the HGR temperature.

Catalyst stability was checked by consecutive additions of the same specified amount of $NaBH_4$ as soon as the H_2 evolution of the previous run ceased, measuring againg the released gas with the gas burette. Five consecutive runs of catalytic HGRs with the same catalyst sample were carried out at room temperature. Upon completion of the last HGR of the stability test, the QT-x was separated from the reaction mixture by centrifugation and washed several times with deionized water and then dried at 100 °C under vacuum for 10 h. It was then used for PXRD and ICP analyses.

Results and discussion

Characterization

Cobalt based TMU-10 MOF, $[Co_6(oba)_5(OH)_2(H_2O)_2(DMF)_4]_n\cdot 2DMF$ was synthesized in large scale by mixing of $Co(NO_3)_2\cdot 6H_2O$ and H_2oba as indicated in the experimental section. This MOF is based on hexanuclear secondary building units (SBU), $Co_6(CO_2)_{10}(O)_2(O)_4$ (Fig. 1), with pores running along the b- (6.2 × 6.1 Å) and c-axes (9.6 × 4.3 Å). The structure has 32.7 % void space per unit cell (Fig. 1). The SBU contains three crystallographically independent six coordinated Co (II) centers. All cobalt (II) centers are bound to six oxygen atoms from oba ligands, μ_3-O atom of OH^- anion, oxygen atom of H_2O or DMF molecules (Fig. 1).

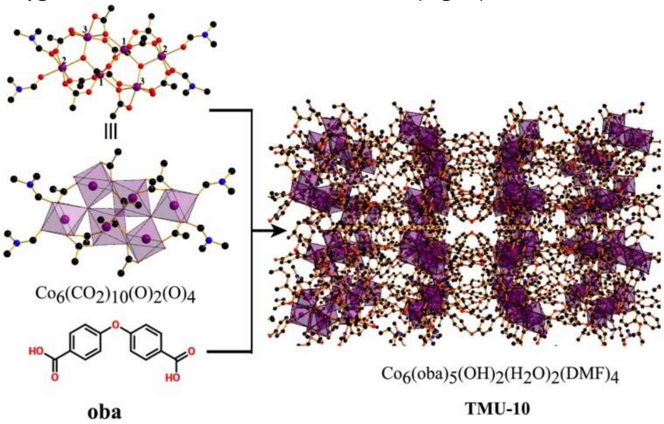

Fig. 1 Single-crystal X-ray structure of TMU-10. Color code: O, red; N, blue; C, black; and Co, purple and purple polyhedra.

Based on TGA measurements, thermal calcination should produce the partial TMU-10 deligandation, probably with the result of generation of pores and creation of unsaturated inorganic nodes. For this purpose, eight different temperatures (i.e. 100, 150, 200, 250, 300, 350, 400, and 700 °C) were selected for thermal treatment of TMU-10 under air for 1 h in order to remove solvent and a fraction of ligands. At temperatures up to 150 °C, two DMF guest molecules and one water bonded molecule from each of Co(3) centers were removed from the framework making five coordinate Co(3) centers. Upon increasing the temperature at 200 °C, two DMF coordinated molecules to either of Co(2) centers were removed forming four coordinated Co(2) centers. At 300 °C, two μ_3-O atoms of OH^- anion in the framework were detached resulting in Co(1), Co(2) and Co(3) with coordination numbers of five, three, and four, respectively (Fig. S3).

The morphologies of parent TMU-10 and QT-300 samples were investigated using the FE-SEM. TMU-10 sample is comprised of nanoparticles (Fig. S4a). Thermal treatment at 300 °C causes agglomeration of the TMU-10 particles into larger particles observed for QT-300 sample (Fig. S4b).

The evolution of the cobalt atomic valence states from TMU-10 to QT-300 was determined by XPS (Fig. 2). The XP spectrum of TMU-10 exhibits the peaks of Co $2p_{3/2}$ and Co $2p_{1/2}$ located at 780.5 eV and 796 eV with corresponding intense satellite centered at 786.3 eV and 803 eV, respectively, which are attributed to Co(II).[47] In the case of QT-300 sample, four new peaks appeared at 779.6, 782.9, 789, and 804.5 eV. The curve-fitting reveals that these new peaks can be ascribed to Co(III) $2p_{3/2}$ main peak, Co(II) in tetrahedral sites and two shake up satellites for Co(III), respectively along with the decrease in the previous peak intensities of octahedral Co(II). [48, 49] These results confirm that after deligandation a portion of Co(II) centers was converted to Co(III) along with creating Co(II) in tetrahedral sites.

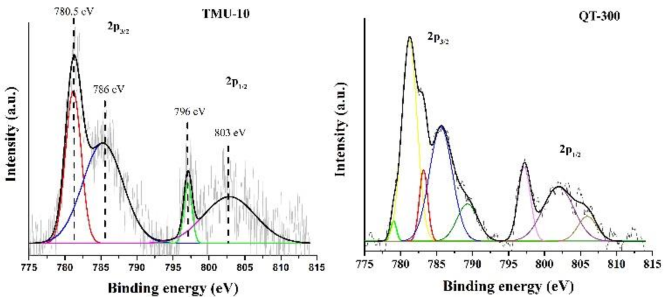

Fig. 2 XP spectra of the Co 2p peaks for TMU-10 and QT-300 samples and their best deconvolution to individual components.

The variable temperature PXRD of TMU-10 demonstrates that the crystal structure is retained up to 300 °C and broadening of the diffraction peaks around 6° –7° can reflect the partial deligandation of TMU-10 (Fig. 3). When the temperature rises to 350 °C, the characteristic peaks of TMU-10 significantly decrease in intensity showing high degrees of structural collapse. The peaks corresponding to TMU-10 completely disappear at 400 °C, while in turn Co_3O_4 related diffraction peaks appear (JCPDS No. 42-1467) implying the complete decomposition of the TMU-10 framework at this temperature.

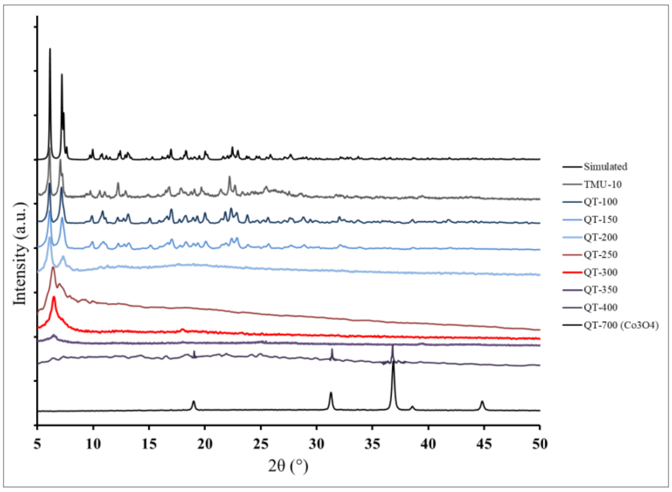

Fig. 3 Comparison of PXRD patterns for simulated TMU-10, TMU-10 and QT-x.

The evolution of porosity upon thermal treatment of TMU-10 was investigated by N_2 adsorption isotherms collected at 77 K for both TMU-10 and QT-300 (Fig. 4). The data show that BET surface area and total pore volume increase from 8.2 m^2/g and 0.023 cm^3/g for TMU-10 to 38.8 m^2/g and 0.157 cm^3/g in the case of QT-300, respectively (Table S1). The increase in the surface area and pore volume of QT-300 in comparison with TMU-10 can be attributed to the occurrence of partial deligandation and creation of vacant sites in the quasi MOF. Also, total mesoporous volume increases about 7.5 times from 0.019 cm^3/g for TMU-10 to 0.142 cm^3/g for QT-300, accompanied by a considerable growth in the adsorption at high relative pressures ($P/P_0 > 0.9$) indicating the presence of large cavities. Analysis of the BJH pore size distribution also corroborates the increase of pore width in QT-300 caused by thermal treatment (Fig. 4). Therefore, the structural changes caused by the thermal treatment of TMU-10 with generation of unsaturated metal sites in both micro- and mesopores should be reflected in an efficient enhancement of the catalytic performance of QT-300 compared to TMU-10.

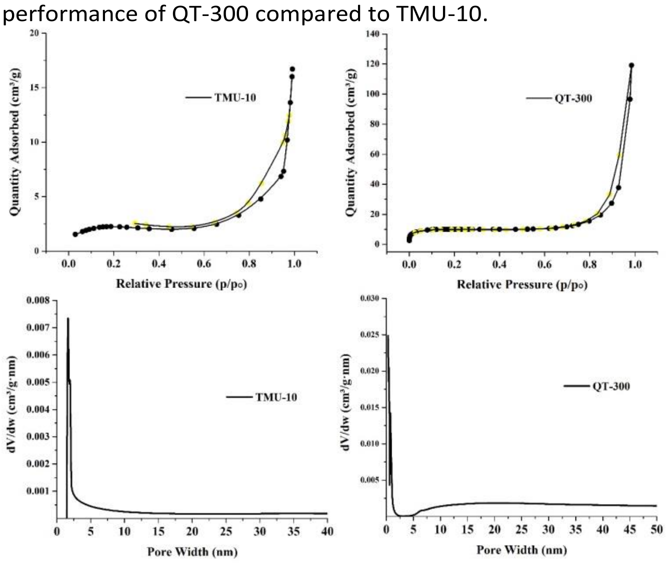

Fig. 4 N_2 isotherms at 77 K and 1 bar and pore size distribution for TMU-10 and QT-300.

The catalytic HGR performance

The turnover frequency (TOF) of the active metal sites, calculated by measuring the H_2 evolution in the $NaBH_4$ hydrolysis was considered as the catalytic parameter to compare the catalytic activity of QT-x vs. the parent TMU-10. The HGRs were carried out in water in absence and/or presence of a proper QT-x catalyst. Various parameters such as different temperature of the thermal treatment, HGR reaction temperature, amount of catalyst, HGR activation energy and adsorption enthalpy and entropy were also investigated.

Influence of the thermal treatment temperature

The effect of the thermal treatment temperature on catalytic HGR of the quasi MOFs, i.e. QT-100, QT-150, QT-200, QT-250, QT-300, QT-350 and QT-400 was investigated for the hydrolysis of $NaBH_4$ at room temperature (Table 1 and Fig. S5). The HGR in the absence of catalyst (self-hydrolysis of $NaBH_4$) was measured first and, as expected, was low, resulting in 60 mL within 60 min. As observed, only a small percentage of the theoretical H_2 amount was released by self- hydrolysis of $NaBH_4$ at room temperature, [50] while the HGR was accelerated using QT-x catalysts (Fig. S5). TMU-10 shows a substantially higher HGR than the self-hydrolysis of $NaBH_4$. Importantly, QT-x samples arising from the thermal treatment of TMU-10 exhibit much higher TOF values than those of parent (TMU-10) and related cobalt oxide (Co_3O_4) for the room temperature HGR. For instance, the TOF value in presence of QT-250 and QT-300 catalysts, determined at 20 and 10 min reaction time, respectively, increased to 5000 and 13333 mL min^{-1} g^{-1}. The TOFs in presence of QT-250 and QT-300 catalysts were respectively 12.5 and 33.3 times higher than that of TMU-10 at 25 °C. When the treatment temperature was further increased, the TOF values of the resulting catalysts were all significantly decreased. These data demonstrate that both the pore structure and the content of coordinatively unsaturated metal sites changed and were found to be the dominant factors affecting the HGR performance. The QT-300 catalyst shows notably the highest catalytic HGR activity among other QT-x catalysts probably due to the micro-/mesoporosity and the high density of open cobalt sites in which cobalt centers can be better reduced. In the case of QT-300 catalyst, the TOF was 2.4 times higher than QT-250 with a two-fold decrease in reaction time for complete $NaBH_4$ decomposition. The HGR performance drastically diminishes from 350 to 700 °C and the lowest TOF value was measured for QT-350 at a longer time.

These observations can be explained based on the TGA, XPS and XRD data. At deligandation temperature of 150 °C, Co (3) center in the framework loses a coordinated H_2O molecule and coordinatively unsaturated positions on the cobalt increases HGR performance compared to the QT-100. In the case of QT-200 sample, there are two unsaturated cobalt centers corresponding to one Co(3) (coordination number, C.N= 5) and a Co(2) (C.N=4) due to loss of two coordinated DMF molecules. In the case of QT-250, OH ligand bridging three cobalt centers, Co(1), Co(2) and Co(3), is partially removed which causes the good HGR performance of the sample prepared at 250 °C. However, the complete removal of OH bridging ligand occurring for QT-300 is responsible for the generation of three unsaturated cobalt centers (1), (2) and (3) and simultaneous existence of meso- and micropores (in accordance with type I and IV curves), resulting in the optimal catalytic activity. At higher treatment temperatures, a major part of the TMU-10 framework collapsed, causing a dramatic decline in TOF values. As the temperature increases, Co_3O_4 phase appears which is responsible for HGR in QT-400 sample. According to the above data, QT-300 sample was chosen as the best catalyst and it was subsequently employed for further experimental HGR studies.

The density and types of acidic sites in parent TMU-10 and QT-300 catalysts were also estimated using NH_3-TPD (Fig. 5 and Table 2). Two NH_3 desorption peaks of TMU-10 appeared at 174 °C and 313 °C attributable to low and medium acidity strength, respectively. In the case of QT-300, these peaks appeared at 174 °C and 331°C. TPD results demonstrated that QT-300 catalyst adsorbed much more ammonia compared with parent TMU-10. In other words, structural transformation of TMU-10 at 300 °C leads to an increase in total acidity of about 3 times, most of which is related to the increase in medium acid sites. Accordingly, the QT-300 catalyst exhibits the highest catalytic activity in the $NaBH_4$ hydrolysis.

Table 1. TOF values measured for the hydrolysis of $NaBH_4$ catalyzed by various Q-MOFs.

Q-MOF	Time (min)	TOF (ml.min^{-1}g^{-1})
No catalyst	60	*1
QT-100	180	400
QT-150	180	526
QT-200	180	644
QT-250	20	5000
QT-300	10	13333
QT-350	360	300
QT-400	360	385
QT-700**	360	426

Experimental conditions: Catalyst mass = 1.5 mg, [$NaBH_4$] = 125 mM and T= 25°C. *: (mL.min^{-1})** Co_3O_4.

Table 2. The amount of acidic sites in TMU-10 and QT-300 catalysts according to NH_3-TPD experiments.

Catalyst	weak acid		Strong acid		Total acidity (mmolg^{-1})
	Peak position (°C)	Value (mmolg^{-1})	Peak position (°C)	Value (mmolg^{-1})	
TMU-10	174	5.5	313	5.3	10.8
QT-300	174	0.6	331	31.8	32.4

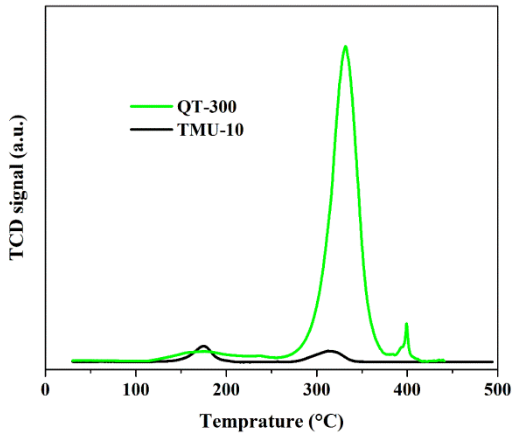

Fig. 5 Temperature-programmed desorption of NH_3 from TMU-10 and QT-300 catalysts.

Effect of QT-300 catalyst dosage on HGR performance

Since catalyst dosage is an important parameter controlling for HGR controlling the rate of $NaBH_4$ hydrolysis, the effect of various amounts of QT-300 catalyst was also investigated at room temperature (Table S2 and Fig. S6). In principle, TOF values should be constant regardless the amount of catalysts. However, in the present case it was observed that with 1 mg of QT-300 catalyst, H_2 volume reaches 120 ml within 15 min with the corresponding TOF at about 8000 ml min^{-1} g^{-1}. By increasing the amount of QT-300 to 2 mg, TOF increases from 8000 to 15625 ml min^{-1} g^{-1} within a shorter time of about 8 min. However, above 2 mg of QT-300 catalyst, TOF did not increase significantly and remained almost constant. Hence, 2 mg is chosen as the optimal amount of QT-300 catalyst in all experiments. This behavior could indicate that a fraction of the initial material act as sacrificial agent, becoming poisoned/decomposed by the reaction medium. Thus, it could be that spontaneous formation of the $NaBO_2$ by-product at the initial times of HGR blocks some catalytic sites on QT-300. Upon addition of subsequent catalyst amounts, the decomposed material becomes negligible and a constant TOF value is reached.

The generated H_2 volume versus time for various amounts of QT-300 catalyst was also investigated (Fig. S7). The logarithmic plot of the H_2 generation rate on the concentration of QT-300 catalyst shows a slope of 1.262, indicating that the catalytic hydrolysis of $NaBH_4$ by QT-300 follows a quasi-first-order kinetics in catalyst concentration.

Effect of $NaBH_4$ concentration on HGR performance

Since the amount of $NaBH_4$ could affect HGR, the dosage of $NaBH_4$ in the solution was also examined at 25 °C (Fig. S8). Upon adding higher $NaBH_4$ concentrations from 125 mM to 250 mM, HGR values varied significantly from 250 mL to 480 mL within 12 min. For all three $NaBH_4$ concentrations, the HGR curves initially overlap with each other and thus HGR in the three cases is almost the same. As discussed earlier when commenting the trend on the TOF, this behavior could reflect the spontaneous formation of $NaBO_2$ at initial HGR times, deactivating some catalytic sites of QT-300.Nevertheless, the catalytic HGR in presence of QT-300 is very stable and impressive in a high concentration of $NaBH_4$, indicating a superiority of QT-300 catalyst respect to other reported catalytic systems for the same HGR.

Also, the HGR kinetics can be considered as first order respect $NaBH_4$ concentration, deduced from the slope of the logarithmic plot of HGR versus $NaBH_4$ concentration (0.771) (Fig. S9).

Effect of temperature on HGR performance over QT-250

The influence of the temperature on the HGR catalyzed by QT-300 was also evaluated (Fig. 6). The activation energy (E_a) was calculated in accordance with the Arrhenius equation (Eq.2).

The activation energy of catalytic HGR in presence of QT-300 catalyst was estimated as 56.8 kJ/mol (Fig. S10) which is in the range of most cobalt-based reported catalysts for $NaBH_4$ hydrolysis (Table 3). The relatively low activation energy probably results from the synergistic effects of open active cobalt sites and simultaneous existence of both meso- and micropores which can react with water and $NaBH_4$. In other words, QT-300 catalyst provides more active sites with easy mass transfer and diffusion of the substrate and product molecules due to the hierarchical porosity during the HGR.

The thermodynamic studies of catalytic HGR were also carried out at different temperatures using the Eyring equation (Eq.3):

$$\ln\left(\frac{k_{app}}{T}\right) = -\frac{\Delta H^{\#}}{RT} + \frac{\Delta S^{\#}}{R} \quad (3)$$

$$\Delta G° = \Delta H° - T\Delta S° \quad (4)$$

where ΔH° and ΔS° are the change in the enthalpy (J/mol) and the entropy (J/mol K) respectively.

The enthalpy and the entropy values obtained were 54.25 kJ/mol and 214.3 (j/mol K), respectively (Fig. S11). The Gibbs free-energy of activation ($\Delta G^{\#}$) was also estimated and summarized in Table 4. Regarding the negative $\Delta G^{\#}$ values, the HGR over QT-300 catalyst takes place spontaneously in the range of 298-313 K and is enhanced by increasing the temperature. Moreover, the increased temperature and the positive ΔH° values show that HGR on active cobalt sites of QT-300 catalyst is an endothermic process that results in an increased disorder (ΔS°>0).

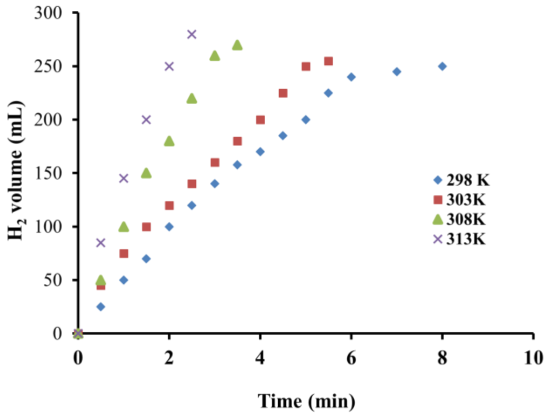

Fig. 6 Catalytic HGR in the presence of QT-300 catalyst at various temperatures. Reaction conditions: catalyst mass = 2 mg and $[NaBH_4]$ = 125 mM.

Table 3. Comparison of activation energies (E_a) of HGR from $NaBH_4$ hydrolysis for various Co-based catalysts.

Catalyst	TOF ($mL.min^{-1}.g^{-1}$)	E_a (kJ/mol)	Temperature range (°C)	Ref.
CoNPs@ZIF-8	19476[a] 35718[a]	62.9	30 40	14
CoB/ZIF-8	506	57.7	35	51
Co-ZIF-9	3642	-	40	52
Co-Co_3O_4@C-II derived from pyrolysis of Co-MOFs@GP (glucose polymer)	5360 ~ 10938[b]	37.12	25 55	53
Co@C derived from ZIF-67	2030[c] 4900[d]	[c]64.3 [d]25.8	50	54
Co@CoOx@C Derived from Co-MOF	2140	23.3	30-55	46
QuasiTMU-10 (QT-300)	15625 44800	56.8	25 40	This study

[a] The TOF(s) is related to the surface atom number of the cobalt NPs. [b] Calculated from Fig. 5d in Ref. 49. [c] without NaOH and [d] with NaOH.

Table 4. Thermodynamic parameters of HGR on QT-300 at various temperatures.

T (K)	ΔG° (kJ/mol)	ΔH° (kJ/mol)	ΔS° (J/mol K)	R^2
298	-63.80	54.25	214.3	0.984
303	-64.90			
308	-65.95			
313	-67.02			

Possible HG Mechanism over QT-300

The catalytic $NaBH_4$ hydrolysis follows the Langmuir-Hinshelwood (LH) model[14, 55] in which two reactants are adsorbed on the solid catalyst. In the LH mechanism, the adsorption and desorption rates are much greater than the surface reaction rate on catalyst. Thus, the chemical reaction of the two adsorbed molecules, rather than diffusion, plays a role in the rate-determining step (RDS). It has also been found that one of the hydrogen atoms in H_2 comes from water and another from $NaBH_4$.[56] Based on the observation of a kinetic isotope effect, the O-H bond cleavage of water has been proposed to occur in the RDS. To gain information of the HGR catalyzed by QT-300, further investigation was performed on the kinetic isotope effect to determine if also H2O hydrolysis is involved in the RDS of the $NaBH_4$ hydrolysis promoted by QT-300 catalyst. For this purpose, the HGR in presence of QT-300 catalyst was investigated in the $NaBH_4$+D_2O system (Fig. 7). The results clearly indicate an important primary kinetic isotope effect due to very high value of k_H to k_D (k_H/k_D= 7.5). This observation supports that the O-H bond cleavage of water molecule is a major process involved in the RDS and HGR obeys the LH mechanism.

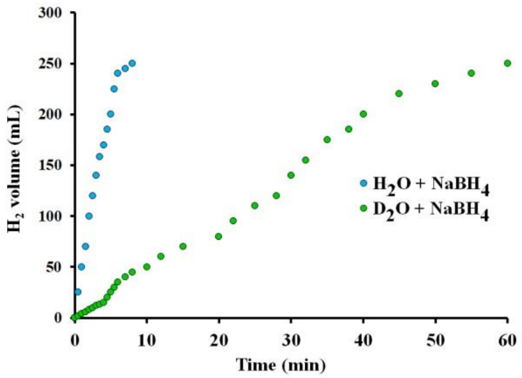

Fig. 7 Temporal profiles of H_2 evolution measured for the $NaBH_4$ hydrolysis in two systems of H_2O and D_2O over 2 mg of QT-300 catalyst at 25 °C.

In the case of QT-300 catalyst, open cobalt active sites as Lewis acids can promote the adsorption of BH_4^- species and water molecules on the catalyst surface. Also, QT-300 catalyst provides more active sites with easy mass transfer through the catalyst matrix. Moreover, hierarchical porosity facilitates the entry and diffusion of the substrate and product molecules during the catalytic cycles. As mentioned above, the O-H bond cleavage of H_2O exactly happens in the RDS in the presence of QT-300. Generally, there is the hydrogen bonding between BH_4^- and an acidic hydrogen atom of H_2O. Under ambient conditions and without any catalyst, derivation of two hydrogen atoms from precursors to produce H_2 is very slow. The transfer of two hydrogen atoms to the cobalt atom takes places in presence of a proper catalyst. Then a cobalt-dihydride intermediate and BH_3OH^- species are formed. Finally, the product of H_2 releases from the QT-300 surface during catalytic cycles (Scheme 1).

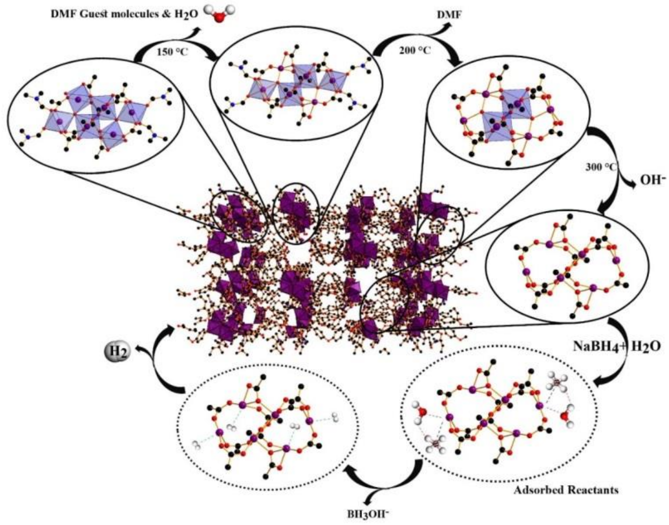

Scheme 1. Simplified illustration of the effect of thermal treatment on TMU-100 structure and proposed HGR mechanism over QT-300 catalyst.

Reusability of QT-300 catalyst

In order to examine the reusability of the catalyst, the same sample of QT-300 was submitted to six catalytic runs. calculating the TOF for each run. The superior catalytic HGR activity and excellent stability of QT-300 were assessed by observing a nearly constant initial activity after being used up to six times (Fig. S12a). The framework of the QT-300 catalyst remained unaltered as confirmed by comparison of the XRD pattern of fresh and six times-used QT-300 (Fig. S12b), confirming the structural stability of the catalyst. Moreover, ICP measurements established the absence of a significant amount of cobalt in the supernatant after each cycle, showing that no cobalt leaching from the solid catalyst into the aqueous media happens. These results indicate that the quasi cobalt-based MOF is stable and can be reused in the catalytic HGR from $NaBH_4$ hydrolysis.

Conclusions

Post-synthetic pore engineering on a cobalt based metal-organic framework (TMU-10), $[Co_6(oba)_5(OH)_2(H_2O)_2(DMF)_4]_n$·2DMF has been carried out via controlled thermolysis treatments in air atmosphere at different temperatures in the range of 100-700 °C. The quasi MOFs were subsequently employed for hydrogen generation by catalytic hydrolysis of $NaBH_4$. The hydrolysis of $NaBH_4$ over quasi catalysts was investigated as a function of the deligandation temperature, catalyst dosage, $NaBH_4$ concentration, and reaction temperature. The catalytic performance exhibited obvious changes with the variation of the deligandation temperature. The maximum turnover frequency was observed in the presence of quasi TMU-10 calcined at 300 °C with the activation energy of about 56.8 kJ mol^{-1}. The synergistic effects of the uniform and extended distribution of more acidic sites on cobalt nodes across the framework, avoidance of particle agglomeration, simultaneous existence of micro- and mesopores (types I and IV), conversion of a portion of Co(II) centers to Co(III), and creation of Co(II) in tetrahedral sites are responsible for this enhanced catalytic performance. Further investigation of the $NaBH_4$+D_2O system hydrolysis shows a primary kinetic isotope effect indicating that the O-H bond cleavage of water molecule occurs in the rate determining step. This study illustrates once again the role that structural defects can play in catalysis and the simplicity of the thermal treatment can be readily extensible to the preparation of other quasi MOF catalysts for H_2 generation process from hydrogen storage compounds targeting to its industrial application.

Acknowledgements

Support of this investigation by Arak University is gratefully acknowledged.

Notes and references

1. T. Hügle, M. Hartl and D. Lentz, The Route to a Feasible Hydrogen-Storage Material: MOFs versus Ammonia Borane, *Chem. Eur. J.*, 2011, **17**, 10184-10207.
2. B. Zhu, R. Zou and Q. Xu, Metal–Organic Framework Based Catalysts for Hydrogen Evolution, *Advanced Energy Materials*, 2018, **8**, 1801193.
3. J. N. Armor, The multiple roles for catalysis in the production of H2, *Appl. Catal., A*, 1999, **176**, 159-176.
4. C. L. Muhich, B. D. Ehrhart, I. Al-Shankiti, B. J. Ward, C. B. Musgrave and A. W. Weimer, A review and perspective of efficient hydrogen generation via solar thermal water splitting, *WIREs Energy and Environment*, 2016, **5**, 261-287.
5. N. A. Bahari, W. N. R. Wan Isahak, M. S. Masdar and Z. Yaakob, Clean hydrogen generation and storage strategies via CO2 utilization into chemicals and fuels: A review, *International Journal of Energy Research*, 2019, **43**, 5128-5150.
6. J. Joy, J. Mathew and S. C. George, Nanomaterials for photoelectrochemical water splitting – review, *Int. J. Hydrogen Energy*, 2018, **43**, 4804-4817.
7. C. Gomes Silva, I. Luz, F. X. Llabrés i Xamena, A. Corma and H. García, Water Stable Zr–Benzenedicarboxylate Metal–Organic Frameworks as Photocatalysts for Hydrogen Generation, *Chem. Eur. J.*, 2010, **16**, 11133-11138.
8. C. Gomes Silva, R. Juárez, T. Marino, R. Molinari and H. García, Influence of Excitation Wavelength (UV or Visible Light) on the Photocatalytic Activity of Titania Containing Gold Nanoparticles for the Generation of Hydrogen or Oxygen from Water, *J. Am. Chem. Soc.*, 2011, **133**, 595-602.
9. L. Yuan, C. Han, M.-Q. Yang and Y.-J. Xu, Photocatalytic water splitting for solar hydrogen generation: fundamentals and recent advancements, *Int. Rev. Phys. Chem.*, 2016, **35**, 1-36.
10. H. Ahmad, S. K. Kamarudin, L. J. Minggu and M. Kassim, Hydrogen from photo-catalytic water splitting process: A review, *Renewable and Sustainable Energy Reviews*, 2015, **43**, 599-610.
11. C. Xing, Y. Liu, Y. Su, Y. Chen, S. Hao, X. Wu, X. Wang, H. Cao and B. Li, Structural Evolution of Co-Based Metal Organic Frameworks in Pyrolysis for Synthesis of Core–Shells on Nanosheets: Co@CoOx@Carbon-rGO Composites for Enhanced Hydrogen Generation Activity, *ACS Appl. Mater. Interfaces*, 2016, **8**, 15430-15438.
12. B. Chen, S. Chen, H. A. Bandal, R. Appiah-Ntiamoah, A. R. Jadhav and H. Kim, Cobalt nanoparticles supported on magnetic core-shell structured carbon as a highly efficient catalyst for hydrogen generation from NaBH4 hydrolysis, *Int. J. Hydrogen Energy*, 2018, **43**, 9296-9306.
13. S. Roy, P. Pachfule and Q. Xu, High Catalytic Performance of MIL-101-Immobilized NiRu Alloy Nanoparticles towards the Hydrolytic Dehydrogenation of Ammonia Borane, *Eur. J. Inorg. Chem.*, 2016, **2016**, 4353-4357.
14. C. Luo, F. Fu, X. Yang, J. Wei, C. Wang, J. Zhu, D. Huang, D. Astruc and P. Zhao, Highly Efficient and Selective Co@ZIF-8 Nanocatalyst for Hydrogen Release from Sodium Borohydride Hydrolysis, *Chemcatchem*, 2019, **11**, 1643-1649.
15. R. Retnamma, A. Q. Novais and C. M. Rangel, Kinetics of hydrolysis of sodium borohydride for hydrogen production in fuel cell applications: A review, *Int. J. Hydrogen Energy*, 2011, **36**, 9772-9790.
16. Ö. Metin, Ş. Şahin and S. Özkar, Water-soluble poly(4-styrenesulfonic acid-co-maleic acid) stabilized ruthenium(0) and palladium(0) nanoclusters as highly active catalysts in hydrogen generation from the hydrolysis of ammonia–borane, *Int. J. Hydrogen Energy*, 2009, **34**, 6304-6313.
17. N. Sieffert and M. Bühl, Hydrogen Generation from Alcohols Catalyzed by Ruthenium−Triphenylphosphine Complexes: Multiple Reaction Pathways, *J. Am. Chem. Soc.*, 2010, **132**, 8056-8070.
18. P. Dai, J. Xie, M. T. Mayer, X. Yang, J. Zhan and D. Wang, Solar Hydrogen Generation by Silicon Nanowires Modified with Platinum Nanoparticle Catalysts by Atomic Layer Deposition, *Angew. Chem. Int. Ed.*, 2013, **52**, 11119-11123.
19. Y.-J. Yuan, Z.-T. Yu, D.-Q. Chen and Z.-G. Zou, Metal-complex chromophores for solar hydrogen generation, *Chem. Soc. Rev.*, 2017, **46**, 603-631.
20. C. Wei, H. Hou, E. Wang and M. Lu, Preparation of a Series of Pd@UIO-66 by a Double-Solvent Method and Its Catalytic Performance for Toluene Oxidation, *Materials*, 2020, **13**, 88.
21. M. Y. Masoomi, A. Morsali, A. Dhakshinamoorthy and H. Garcia, Mixed-Metal MOFs: Unique Opportunities in Metal–Organic Framework (MOF) Functionality and Design, *Angew. Chem. Int. Ed.*, 2019, **58**, 15188-15205.
22. M. Bagheri and M. Y. Masoomi, Sensitive Ratiometric Fluorescent Metal-Organic Framework Sensor for Calcium Signaling in Human Blood Ionic Concentration Media, *ACS Appl. Mater. Interfaces*, 2020, **12**, 4625-4631.
23. M. Bagheri, M. Y. Masoomi and A. Morsali, A MoO3–Metal–Organic Framework Composite as a Simultaneous Photocatalyst and Catalyst in the PODS Process of Light Oil, *ACS Catal.*, 2017, DOI: 10.1021/acscatal.7b02581, 6949-6956.
24. A. Dhakshinamoorthy, A. M. Asiri and H. García, Metal–Organic Framework (MOF) Compounds: Photocatalysts for Redox Reactions and Solar Fuel Production, *Angew. Chem. Int. Ed.*, 2016, **55**, 5414-5445.

25. A. Dhakshinamoorthy, Z. Li and H. Garcia, Catalysis and photocatalysis by metal organic frameworks, *Chem. Soc. Rev.*, 2018, **47**, 8134-8172.
26. M. Lu, H. Hou, C. Wei, X. Guan, W. Wei and G.-S. Wang, Preparation of Quasi-MIL-101(Cr) Loaded Ceria Catalysts for the Selective Catalytic Reduction of NOx at Low Temperature, *Catalysts*, 2020, **10**, 140.
27. M.-L. Hu, M. Y. Masoomi and A. Morsali, Template strategies with MOFs, *Coord. Chem. Rev.*, 2019, **387**, 415-435.
28. A. Bavykina, N. Kolobov, I. S. Khan, J. A. Bau, A. Ramirez and J. Gascon, Metal–Organic Frameworks in Heterogeneous Catalysis: Recent Progress, New Trends, and Future Perspectives, *Chem. Rev.*, 2020, **120**, 8468-8535.
29. J. Kim, S.-N. Kim, H.-G. Jang, G. Seo and W.-S. Ahn, CO 2 cycloaddition of styrene oxide over MOF catalysts, *Appl. Catal., A*, 2013, **453**, 175-180.
30. M. Bagheri, M. Y. Masoomi and A. Morsali, High organic sulfur removal performance of a cobalt based metal-organic framework, *J. Hazard. Mater.*, 2017, **331**, 142-149.
31. C. Xu, R. Fang, R. Luque, L. Chen and Y. Li, Functional metal–organic frameworks for catalytic applications, *Coord. Chem. Rev.*, 2019, **388**, 268-292.
32. P. Dong, H. Wang, W. Liu, S. Wang, Y. Wang, J. Zhang, F. Lin, Y. Wang, C. Zhao, X. Duan, S. Wang and H. Sun, Quasi-MOF derivative-based electrode for efficient electro-Fenton oxidation, *J. Hazard. Mater.*, 2021, **401**, 123423.
33. H. Yang, F. Peng, C. Dang, Y. Wang, D. Hu, X. Zhao, P. Feng and X. Bu, Ligand Charge Separation To Build Highly Stable Quasi-Isomer of MOF-74-Zn, *J. Am. Chem. Soc.*, 2019, **141**, 9808-9812.
34. N. Tsumori, L. Chen, Q. Wang, Q.-L. Zhu, M. Kitta and Q. Xu, Quasi-MOF: Exposing Inorganic Nodes to Guest Metal Nanoparticles for Drastically Enhanced Catalytic Activity, *Chem*, 2018, **4**, 845-856.
35. L. Fan, F. Zhao, Z. Huang, B. Chen, S.-F. Zhou and G. Zhan, Partial deligandation of M/Ce-BTC nanorods (M = Au, Cu, au-cu) with “Quasi-MOF” structures towards improving catalytic activity and stability, *Appl. Catal., A*, 2019, **572**, 34-43.
36. M. R. Ryder, J. Maul, B. Civalleri and A. Erba, Quasi-Harmonic Lattice Dynamics of a Prototypical Metal–Organic Framework, *Adv. Theory Simul*, 2019, **2**, 1900093.
37. A. Corma and H. García, Lewis Acids as Catalysts in Oxidation Reactions: From Homogeneous to Heterogeneous Systems, *Chem. Rev.*, 2002, **102**, 3837-3892.
38. Y. Wen, J. Zhang, Q. Xu, X.-T. Wu and Q.-L. Zhu, Pore surface engineering of metal–organic frameworks for heterogeneous catalysis, *Coord. Chem. Rev.*, 2018, **376**, 248-276.
39. M. Bagheri, A. A. Khodadadi, A. R. Mahjoub and Y. Mortazavi, Highly sensitive gallia-SnO2 nanocomposite sensors to CO and ethanol in presence of methane, *Sens. Actuators, B*, 2013, **188**, 45-52.
40. M. Bagheri, A. A. Khodadadi, A. R. Mahjoub and Y. Mortazavi, Strong effects of gallia on structure and selective responses of Ga2O3–In2O3 nanocomposite sensors to either ethanol, CO or CH4, *Sens. Actuators, B*, 2015, **220**, 590-599.
41. J.-X. Liu, Y. Su, I. A. W. Filot and E. J. M. Hensen, A Linear Scaling Relation for CO Oxidation on CeO2-Supported Pd, *J. Am. Chem. Soc.*, 2018, **140**, 4580-4587.
42. H. Y. Kim, H. M. Lee and G. Henkelman, CO Oxidation Mechanism on CeO2-Supported Au Nanoparticles, *J. Am. Chem. Soc.*, 2012, **134**, 1560-1570.
43. G. Chen, Z. Guo, W. Zhao, D. Gao, C. Li, C. Ye and G. Sun, Design of Porous/Hollow Structured Ceria by Partial Thermal Decomposition of Ce-MOF and Selective Etching, *ACS Appl. Mater. Interfaces*, 2017, **9**, 39594-39601.
44. Y. Shen, L.-W. Bao, F.-Z. Sun and T.-L. Hu, A novel Cu-nanowire@Quasi-MOF via mild pyrolysis of a bimetal-MOF for the selective oxidation of benzyl alcohol in air, *Mater. Chem. Front*, 2019, **3**, 2363-2373.
45. M. Y. Masoomi, M. Bagheri and A. Morsali, Application of Two Cobalt-Based Metal–Organic Frameworks as Oxidative Desulfurization Catalysts, *Inorg. Chem.*, 2015, **54**, 11269-11275.
46. C. Xing, Y. Liu, Y. Su, Y. Chen, S. Hao, X. Wu, X. Wang, H. Cao and B. Li, Structural Evolution of Co-Based Metal Organic Frameworks in Pyrolysis for Synthesis of Core-Shells on Nanosheets: Co@CoOx@Carbon-rGO Composites for Enhanced Hydrogen Generation Activity, *ACS Appl. Mater. Interfaces*, 2016, **8 24**, 15430-15438.
47. T. J. Chuang, C. R. Brundle and D. W. Rice, Interpretation of the x-ray photoemission spectra of cobalt oxides and cobalt oxide surfaces, *Surf. Sci.*, 1976, **59**, 413-429.
48. M. Fantauzzi, F. Secci, M. Sanna Angotzi, C. Passiu, C. Cannas and A. Rossi, Nanostructured spinel cobalt ferrites: Fe and Co chemical state, cation distribution and size effects by X-ray photoelectron spectroscopy, *RSC Adv.*, 2019, **9**, 19171-19179.
49. M. C. Biesinger, B. P. Payne, A. P. Grosvenor, L. W. M. Lau, A. R. Gerson and R. S. C. Smart, Resolving surface chemical states in XPS analysis of first row transition metals, oxides and hydroxides: Cr, Mn, Fe, Co and Ni, *Appl Surf Sci*, 2011, **257**, 2717-2730.
50. Y. Kojima, Y. Kawai, H. Nakanishi and S. Matsumoto, Compressed hydrogen generation using chemical hydride, *J. Power Sources*, 2004, **135**, 36-41.
51. Q. Li, W. Yang, F. Li, A. Cui and J. Hong, Preparation of CoB/ZIF-8 supported catalyst by single step reduction and its activity in hydrogen production, *Int. J. Hydrogen Energy*, 2018, **43**, 271-282.
52. Q. Li and H. Kim, Hydrogen production from NaBH4 hydrolysis via Co-ZIF-9 catalyst, *Fuel Process. Technol.*, 2012, **100**, 43-48.
53. Y. Liu, G. Han, X. Zhang, C. Xing, C. Du, H. Cao and B. Li, Co-Co3O4@carbon core–shells derived from metal–organic framework nanocrystals as efficient hydrogen evolution catalysts, *Nano Res.*, 2017, **10**, 3035-3048.
54. K.-Y. A. Lin and H.-A. Chang, Efficient hydrogen production from NaBH4 hydrolysis catalyzed by a magnetic cobalt/carbon composite derived from a zeolitic imidazolate framework, *Chem Eng J*, 2016, **296**, 243-251.
55. S. Wunder, Y. Lu, M. Albrecht and M. Ballauff, Catalytic Activity of Faceted Gold Nanoparticles Studied by a Model Reaction: Evidence for Substrate-Induced Surface Restructuring, *ACS Catal.*, 2011, **1**, 908-916.
56. P. Brack, S. E. Dann and K. G. U. Wijayantha, Heterogeneous and homogenous catalysts for hydrogen generation by hydrolysis of aqueous sodium borohydride (NaBH4) solutions, *Energy Science & Engineering*, 2015, **3**, 174-188.